



Dynamic 3D scanning as a markerless method to calculate multi-segment foot kinematics during stance phase: Methodology and first application

Inge Van den Herrewegen^a, Kris Cuppens^a, Mario Broeckx^{a,*}, Bettina Barisch-Fritz^d,
Jos Vander Sloten^c, Alberto Leardini^e, Louis Peeraer^{a,b}

^a Mobilab, Thomas More University College, Belgium

^b Department of Rehabilitation Sciences, Faculty of Kinesiology and Rehabilitation Science KU Leuven, Belgium

^c Department of Mechanical Engineering, Faculty of Engineering KU Leuven, Belgium

^d Medical Clinic, Department of Sports Medicine, University of Tuebingen, Germany

^e Movement Analysis Laboratory, Istituti Ortopedici Rizzoli, Italy

ARTICLE INFO

Article history:

Accepted 5 June 2014

Keywords:

Dynamic 3D scanning
4D scanning
Multi-segment foot model
Joint rotations
Foot kinematics

ABSTRACT

Multi-segmental foot kinematics have been analyzed by means of optical marker-sets or by means of inertial sensors, but never by markerless dynamic 3D scanning (D3DScanning). The use of D3DScans implies a radically different approach for the construction of the multi-segment foot model: the foot anatomy is identified via the surface shape instead of distinct landmark points. We propose a 4-segment foot model consisting of the shank (Sha), calcaneus (Cal), metatarsus (Met) and hallux (Hal). These segments are manually selected on a static scan. To track the segments in the dynamic scan, the segments of the static scan are matched on each frame of the dynamic scan using the iterative closest point (ICP) fitting algorithm. Joint rotations are calculated between Sha–Cal, Cal–Met, and Met–Hal. Due to the lower quality scans at heel strike and toe off, the first and last 10% of the stance phase is excluded. The application of the method to 5 healthy subjects, 6 trials each, shows a good repeatability (intra-subject standard deviations between 1° and 2.5°) for Sha–Cal and Cal–Met joints, and inferior results for the Met–Hal joint (> 3°). The repeatability seems to be subject-dependent. For the validation, a qualitative comparison with joint kinematics from a corresponding established marker-based multi-segment foot model is made. This shows very consistent patterns of rotation. The ease of subject preparation and also the effective and easy to interpret visual output, make the present technique very attractive for functional analysis of the foot, enhancing usability in clinical practice.

© 2014 The Authors. Published by Elsevier Ltd. This is an open access article under the CC BY-NC-SA license (<http://creativecommons.org/licenses/by-nc-sa/3.0/>).

1. Introduction

Although research on the biomechanical behavior of the foot is widespread, the origin and impact of the treatment of foot problems are poorly understood. The complex foot structure and huge individual variety among feet foster troublesome analyses, both in research and in clinical practice (Davis, 2004). Methods to

retrieve foot kinematics during walking should thus be accurate and patient-specific.

In biomechanical research, marker-based motion analysis is widely accepted. A variety of marker-based foot models have been developed (Baker, 2006; Deschamps et al., 2011; De Mits et al., 2012; Leardini et al., 2007; Simon et al., 2006). These models divide the foot into several rigid segments and kinematics are calculated as joint rotation angles representing the relative motion of each pair of segments. The foot models differ in the number and choice of segments, and in the way the segments are linked to foot anatomy by marker placement.

However, these marker-based methods show several severe limitations. Firstly, all potential results are limited to the analysis of distinct landmarks. Secondly, skin artifacts create errors in joint rotations up to 8° (Nester et al., 2007) and wrongly located landmarks on the foot result in inter-rater errors (De Mits et al.,

Abbreviations: D3Dscanning, dynamic 3D scanning; Sha, shank; Cal, calcaneus; Met, metatarsus; Hal, hallux; HQS, high-quality stance interval; WSSD, within-subject standard deviation; BSSD, between-subject standard deviation; ICP, iterative closest point; RMS, root mean square

* Correspondence to: Kleinhofstraat 4, 2440 Geel, Belgium.

Tel.: +32 14 80 22 96; fax: +32 14 58 48 59.

E-mail address: mario.broeckx@thomasmore.be (M. Broeckx).

2012; Long et al., 2010; McGinley et al., 2009; Schwarz et al., 2004). Finally, the extensive measurement preparation and relatively complex interpretation of the data limit the usability in clinical practice.

For all aforementioned reasons, finding alternative methods to calculate foot kinematics in a markerless way has been a research topic for the past years. The recently developed dynamic 3D scanners (D3DScanning) provide data of the entire foot surface during walking. Its fast measurement and highly visual output might facilitate the implementation of foot kinematics calculation in clinical practice. Furthermore skin artifacts are reduced as skin movement has little influence on the foot shape. To this date, studies about D3DScanning focus mainly on technical aspects (Blenkinsopp et al., 2012; Coudert et al., 2006; Jezerek and Mozina, 2009). Some studies have applied the technique to quantify dynamic changes in foot dimensions during stance (Fritz et al., 2011, 2013; Kimura et al., 2011; Schmeltzpfenning et al., 2011), but so far no attempts have been made to measure multi-segment foot kinematics.

This study is the first to apply D3DScanning with a focus on the kinematic aspects of foot motion. The aim is to demonstrate the potential of D3DScanning in the development of multi-segment foot models. A multi-segment foot model based on the foot shape is developed to obtain joint rotations between segments during the stance phase of walking. This method is demonstrated on five subjects and the results are compared with previous data on foot kinematics in literature.

2. Materials and methods

2.1. Measurement setup

Data were collected with the multi-scanner-system DynaScan4D (Schmeltzpfenning et al., 2009), consisting of 5 scanner units (ViALUX, Germany) mounted around and below a glass force plate (Fig. 1a). Each unit consists of a camera and a projector. Based on the principle of active triangulation with structured light, a 3D surface point cloud is generated. The entire system is designed to scan the whole foot surface in static and in dynamic situations, the latter during the stance phase of walking and with a frequency between 21 and 49 Hz depending on the chosen binning mode. It was observed that artifacts

like missing parts of the foot surface were common in dynamic scans. The reasons are mainly limitations of the field of view, obstruction by the contralateral swinging leg, or fast moving parts of the foot, especially at heel strike and toe off. With this in mind, the high-quality stance (HQS) interval for each dynamic trial was defined as stance phase minus its first and last 10%. In general, static scans showed better quality, thanks to a higher density of points and fewer artifacts. Fig. 1b demonstrates the quality difference between static and dynamic scans.

2.2. Methodology to calculate foot kinematics

The methodology is summarized in Fig. 2. Four stages can be distinguished and are explained in more detail in the paragraphs below: preprocessing, static segment selection, dynamic segment fitting, and calculation of kinematics. The results are joint rotations between the shank and calcaneus segments (Sha-Cal), between the calcaneus and metatarsus segments (Cal-Met), and between the metatarsus and hallux segments (Met-Hal).

1. Preprocessing

Preprocessing included cleaning up the 3D point clouds by removing noisy points, downsampling the point cloud to 2 mm voxels (in each dimension hence 8 mm³), and the determination of stance phase. Noisy data points mainly come from the background and from reflections. The background includes elements from the environment and the contralateral swinging leg. Therefore, we first subtract an empty scene from the measurements to remove background noise. Afterwards, only the point cloud containing most data points is used for further processing. Additionally, the glass force plate introduces noise due to reflections. To remove this noise, all points below the glass force plate are removed. After the noise removal, the data was spatially downsampled because of the large memory consumption when using the raw data and the high computational time. Finally, we calculated a foot-specific coordinate system from the static scan. This is defined with the transversal plane (Tra) as the ground, the sagittal plane (Sag) perpendicular to this and along the medial side of the foot (determined by the two most medial points), and the frontal plane (Fro) perpendicular to both and through the hindmost point. Positive directions are proximal-to-distal, medial-to-lateral, and upwards. All points of the scan are expressed in this foot-specific coordinate system. Most of the preprocessing was done using Dynascan4D software (Schmeltzpfenning et al., 2009).

2. Segment selection

Since there was no convention about the number and choice of segments in a foot segment model, a new convention was put forward for this particular situation. The selection of each segment was performed on a subject-specific high-quality static scan during full weight bearing. It was a compromise between rigidness, and inclusion of the main shape characteristics. Furthermore, when a poor scan quality complicates the fitting, the boundaries of a segment, as seen from the anatomical point of view, were expanded.

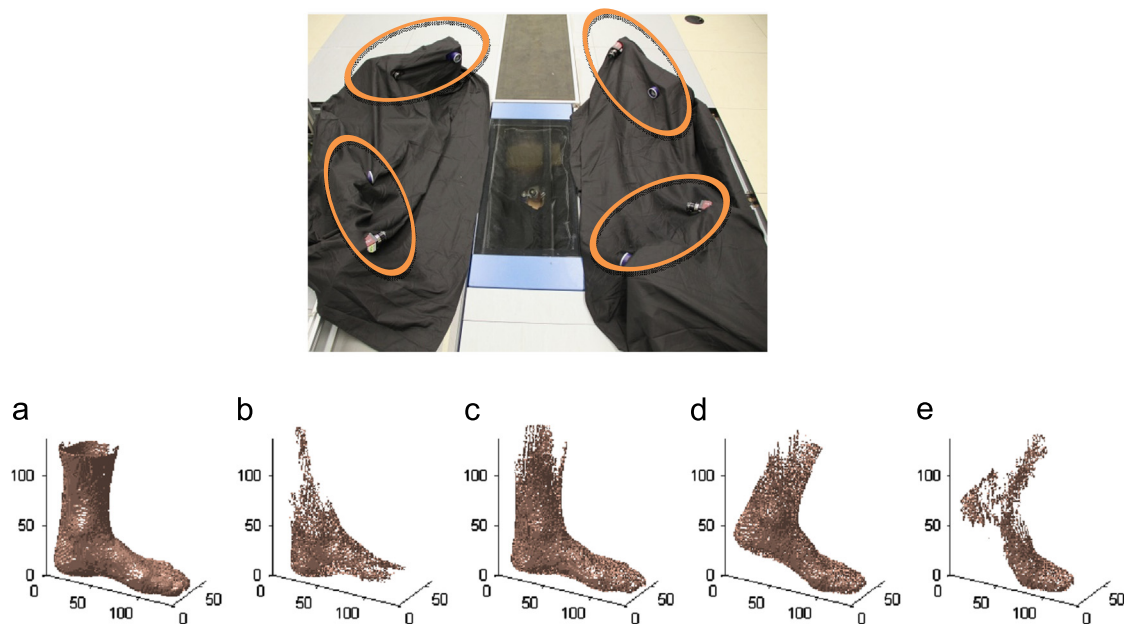


Fig. 1. (a and b) Data collection. a: The measurement setup to capture the entire foot surface, with the four scanners around and one under a glass force plate. The scanners are covered with black anti-reflecting textile. b: Resulting point clouds (after data preprocessing as for Fig. 2); A the static scan; B,C,D,E the frames at 10%, 30%, 80%, and 90% of stance phase of gait. Data in first and last 10% (B and E) are typically of poor quality, therefore high-quality stance (HQS) is defined in the range 10–90% of stance phase.

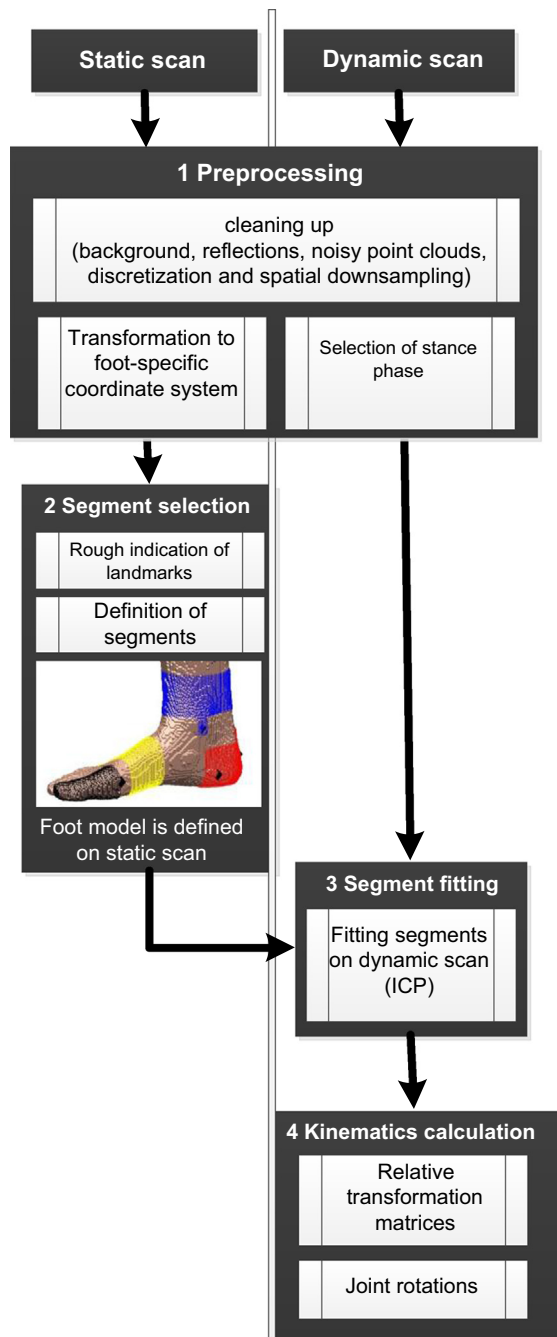


Fig. 2. Workflow to calculate kinematics from the dynamic 3D scans. After preprocessing, four segments are selected on the static scan in full weight-bearing, using an approximate manual indication of landmarks. Subsequently, these segments are fitted on the dynamic scan (walking) resulting in segment trajectories and joint rotation angles.

For example, the calcaneus segment includes a part of the Achilles tendon to increase the number of points in this part of the segment. According to these criteria, four segments were selected (Fig. 4).

- Hallux (Hal): the hallux is defined up to the first metatarsal head to include the characteristic shape of the joint.
- Metatarsus (Met): the metatarsus is defined all around the forefoot from medial to lateral because of its characteristic shape, despite the presence of deformations (Kouchi et al., 2009).
- Calcaneus (Cal): the definition of the calcaneus segment includes the calcaneus area from medial to lateral, and from the plantar surface (despite deformations) till the tuberosity of the calcaneus, with a protrusion toward the Achilles tendon to facilitate fitting.
- Shank (Sha): the definition of the shank segment consists of a strap around the shank and two protrusions at the malleoli, since the lower leg and malleoli constitute the key shape characteristics.

For the realization of above segment selection tasks, first an approximation of the location of certain landmarks was done manually. These points define the borders of the desired segments (Fig. 3). Note that a manually defined offset was used to fully include certain landmarks in the segments such as the malleoli. All borders were aligned with the foot coordinate system (illustrated for the Hal segment in Fig. 4). Table 2 gives an overview of the offset values in the Supplementary appendix.

3. Segment fitting

A fitting algorithm aligned the segments on the dynamic scans, by using the entire point cloud of each segment. The well-established iterative closest point (ICP) algorithm, used previously for similar purposes (Mündermann et al., 2010), was used here. The algorithm is implemented in the version of Wilm et al.¹ with boundary rejection. A fixed number of 50 iterations was used as stopping criterion for the algorithm to determine the final optimal fit (Kjer and Wilm, 2010). ICP defines the segment position in the dynamic frame as the position with minimal root mean square (RMS) error between transformed segment (by translation and rotation) and dynamic frame, resulting in a transformation matrix describing the new position of the segment. To ensure an optimized fit in terms of time and accuracy, the midstance frame (frame where the most points of the plantar surface of the foot touch the ground) was fitted first, and all preceding and subsequent frames were fitted consecutively. The resulting consecutive transformation matrices were multiplied to obtain their transformation matrix with respect to the reference matrix. Supplementary appendix gives a further elaboration on fitting quality.

By downsampling from a resolution of 1 mm in each dimension, to 2 mm (voxels of 8 mm³), we reduced the computational time for segment fitting by almost a factor of 4, i.e. from 2790.12 s to 716.84 s for one typical trial of one typical patient.

4. Calculation of kinematics

The calculation of kinematics (joint rotations) was done in a similar way as with standard marker-based models (Leardini et al., 2007). The inverse multiplication of the segment transformation matrices with their proximal neighbor segment gives the relative transformation matrices: Cal to Sha, Met to Cal, and Hal to Met. The joint rotation angles Sha–Cal, Cal–Met and Met–Hal were calculated as Euler angles, directly derived from the respective relative transformation matrices. Angles of zero degrees correspond to the segment positions as in the static scan.

3. Subjects

Five healthy subjects (3 male and 2 female, free of foot deformities) were scanned. The mean EU shoe size of the sample was 39.5 ± 1.6 , mean age 35.6 ± 12.3 years, mean body length 167.2 ± 7.5 cm, and mean body weight 68.2 ± 9.7 kg. The standardized measurement procedure for each subject included a full weight bearing static scan and subsequently six dynamic trials (32 Hz). The experimental protocol was approved by the ethical committee and a written consent was obtained from each subject prior to participation. The six dynamic scans of each subject were processed as described before. After time normalization over the entire stance phase of the resulting joint rotation angles, the within-subject standard deviation (WSSD) was calculated for each subject, as well as the between-subject standard deviation over all subjects and trials (BSSD).

4. Results

Fig. 5 shows the joint rotations Sha–Cal, Cal–Met and Met–Hal, each represented in the Sag, Fro and Tra plane for the entire stance phase. The intervals outside HQS are colored dark-red.

Fig. 5a shows a representative example (subject 1) with its mean curve and WSSD over 6 trials. Values for WSSD (mean over HQS) for all subjects are reported in Table 1, with their means for the respective angle and subject. WSSD values for Sha–Cal and Cal–Met are between 1° and 2.5° in all planes, while for Met–Hal they are $> 3^\circ$. The repeatability is observed to be subject-dependent, with good WSSD for subjects 1, 2 and 4 ($1.8^\circ \pm 0.1$) and poor WSSD for subjects 3 and 5 ($4.6^\circ \pm 0.7$).

¹ <http://www.mathworks.com/matlabcentral/fileexchange/27804-iterative-closest-point>.

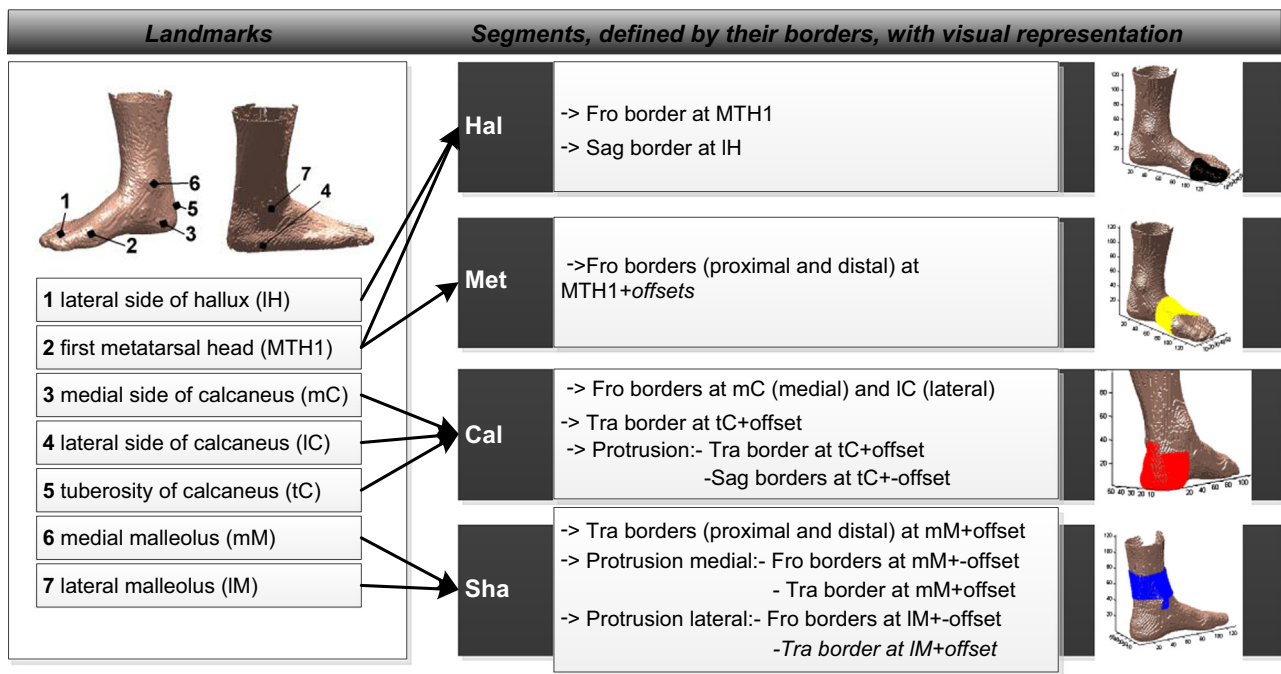


Fig. 3. Indication of landmarks (manually) and subsequent selection of segments (automatically). The segment borders are cut-out of the static scan along coordinate planes Sag, Fro and Tra. See also Fig. 4 for a detailed explanation on the example of the Hal segment.

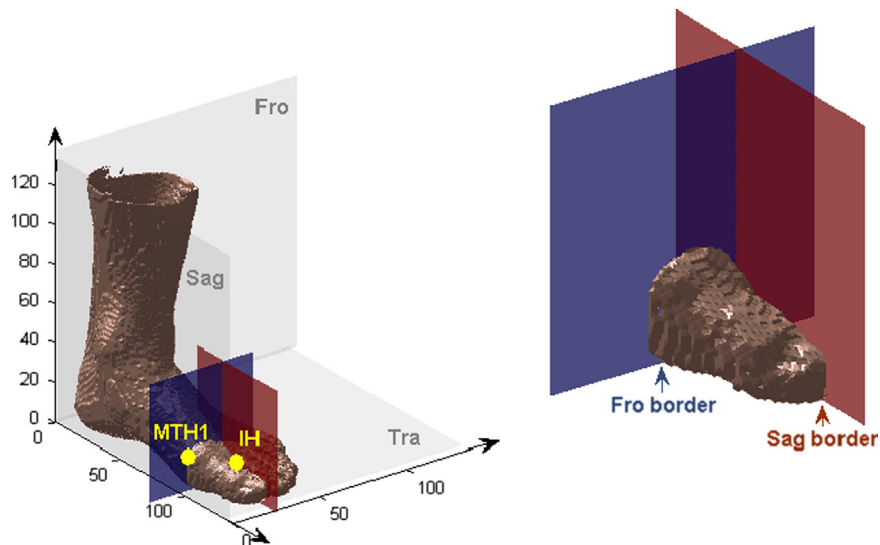


Fig. 4. Detailed explanation of segment selection on the example of the hallux segment (see also Fig. 3). First, the location of MTH1 and IH are manually indicated on the static scan in the foot coordinate system. Secondly, based on these landmarks, the borders of the Hal segment are defined: frontal plane border (blue) at MTH1, and sagittal plane border (red) at IH. Finally, the Hal segment is cut out based on these borders.

Fig. 5b shows the mean curve and BSSD range over all 30 trials. Values for BSSD (mean over HQS) are reported in Table 1. The BSSD values for motions in Sha-Cal and Cal-Met (values between 1.7° and 4°) are larger than their corresponding WSSD values (Table 1). This difference is most pronounced in the Cal-Met Fro motion: WSSD = 1.8° versus BSSD = 4°. The BSSDs in Met-Hal motion are in correspondence with their WSSDs.

All SD ranges feature an hourglass pattern. This is more prominent in some joint rotations than in others, with the largest influence appearing in frontal plane motions of Cal-Met and Met-Hal. Keeping these SDs in mind, several consistent patterns in joint rotations can be observed from the mean curve. Sha-Cal dorsiflexes severely (14°) from

10% ti77ll 70% stance. Also a small eversion rotation (3°) before midstance and small internal rotation (3°) at midstance are observed. At 70% of stance Sha-Cal starts to invert again, though the amount of inversion is not consistent. Cal-Met exhibits generally much smaller rotations. Its main motion is eversion (though not consistent). Also a small dorsiflexion motion (3°) is observed throughout HQS. Results show no consistent transversal plane motion for Cal-Met. In the Met-Hal joint, the toe plantar flexes until midstance, whereafter dorsiflexion motion starts (17°). No consistent transversal plane motion exists in Met-Hal, and its frontal plane motion is not repeatable between subjects. For instance, subject 1 does have a good repeatability for Met-Hal Fro, but shows limited motion.

Table 1

Within-subject standard deviation (WSSD) and between-subject standard deviation (BSSD) for each joint and plane (always mean value over HQS). WSSD was obtained over 6 trials for each subject (1–5). Also mean WSSDs per joint rotation (6th column) and per subject (last row) are reported. BSSD values (last column) are reported per joint rotation as an indicator of repeatability between subjects.

Joint rotations	WSSD (deg)						BSSD (deg)
	Subject 1	Subject 2	Subject 3	Subject 4	Subject 5	Mean all subjects	
Sag Sha-Cal	1.5	1.9	2.2	2.2	3.1	2.2	2.5
Fro Sha-Cal	1.2	1.4	2.1	1.2	1.8	1.5	2.2
Tra Sha-Cal	2.1	1.8	2.0	1.7	2.9	2.1	2.1
Sag Cal-Met	1.4	1.8	1.7	1.5	2.1	1.7	2.0
Fro Cal-Met	1.6	1.3	2.5	1.2	2.6	1.8	4.0
Tra Cal-Met	1.5	1.2	1.8	0.7	1.1	1.3	1.7
Sag Met-Hal	2.4	2.1	4.9	2.1	6.0	3.5	3.2
Fro Met-Hal	3.8	2.3	18.9	3.1	13.2	8.3	7.0
Tra Met-Hal	2.2	1.6	10.5	1.7	4.2	4.0	3.5
Mean all angles	1.9	1.7	5.2	1.7	4.1		

Table 2

Offsets on the landmarks for the selection of the segments, given in mm in the last column. For every segment, the plane in which the boundary lies and the according landmark are given. For the rearfoot and shank segments, extra protrusions are introduced in the segment boundaries. The landmark names are the same as given in Fig. 3.

Segment	Plane	Landmark	Offset (mm)
Hallux	Fro	MTH1	–
	Sag	IH	–
Forefoot	Fro	MTH1	–5
		MTH1	–30
Rearfoot	Fro (med)	mR	–
	Fro (lat)	IR	–
	Tra	tC	+5
Protrusion	Sag	tC	+4
	Tra	tC	+10
Shank	Tra	mM	+15
	Protrusion medial	Fro	+4
		Tra	–4
Protrusion lateral	Fro	IM	+4
			–4
	Tra	IM	–5

5. Discussion

5.1. Repeatability and patterns of joint rotations

The range of WSSDs for Sha-Cal and Cal-Met joints ($1^\circ < \text{WSSD} < 2.5^\circ$) is comparable to previously analyzed values gained by marker-based kinematics (Long et al., 2010). As expected, the between-subject repeatability is poorer than within-subject ($1.7^\circ < \text{BSSD} < 4^\circ$). This difference between WSSD and BSSD indicates the different patterns of motion between subjects, and is most pronounced in the frontal plane motion in the Cal-Met joint: this motion is highly repeatable within subjects (mean WSSD 1.8°) but differs substantially between subjects (BSSD 4°). However, Met-Hal joint rotations appeared to be by far the least repeatable ($\text{WSSD} > 3^\circ$). Inspection of the scans and of the functioning of the method indicates that these errors result from incorrect fitting processes of the Hal segment. The definition of the

boundaries of the hallux segment should thus be reconsidered. The inspection did not reveal errors or other explanations for the poorer repeatability in subjects 3 and 5. The typical hourglass pattern of the SDs seen in Fig. 5 reflects the poorer scan quality towards the start and the end of stance. As a final remark, the present study was limited to five subjects which should be extended in future research.

Comparing the present results with those from an established multi-segment kinematics foot model based on external markers (Leardini et al., 2007), is very encouraging (Fig. 6). Throughout most of HQS, the comparison shows a good trend-wise correspondence. Less corresponding time intervals regarding the joint rotations of the present kinematics, exhibit likewise larger BSSD values. Both techniques share the overall subdivision of the foot segments, but there are other major differences between the techniques which can explain the slightly different patterns of rotation. While the present D3Dscanning kinematics are based on the complete shape of the segments, the other technique is based on corresponding clusters of distinct markers. Furthermore, the 3D joint rotation convention for the present technique is Euler, the hallux is modeled as a 3D segment, and the full-weight bearing stance position is used as reference. The other technique uses Grood and Suntay as the 3D joint rotation convention, the hallux is modeled in 2D, and the half-weight bearing stance position is used as reference. These observations, in addition to the different population analyzed, certainly justify the differences in Fig. 6.

5.2. Development, limitations and improvements to the methodology

The use of D3DScans implies a radically different approach for the construction of the multi-segment foot model. The foot anatomy is identified via the surface shape instead of via distinct landmark points. Because the technique is based on the surface shape, the intrinsic bony movements of the foot may not be reflected in these measurements, but this applies also to skin marker based techniques. Different image processing methods can be applied for the development of such a foot model. This study uses rigid ICP as a first implementation which is appropriate because of its robustness to artifacts in scans (Kjer and Wilm, 2010). Given the deformability of the foot (Kouchi et al., 2009; Okita et al., 2009; Wand et al., 2009), other methods such as non-rigid ICP or deformable shape models might result in a higher reproducibility of the joint rotations calculated from the scan data. However, these methods often lack the ability to deal with artifacts in the scan or the complexity of foot motion. The same applies also to the tracking technique based on 3D optical flow which has been applied to D3Dscans (Van den Herrewegen et al., 2012).

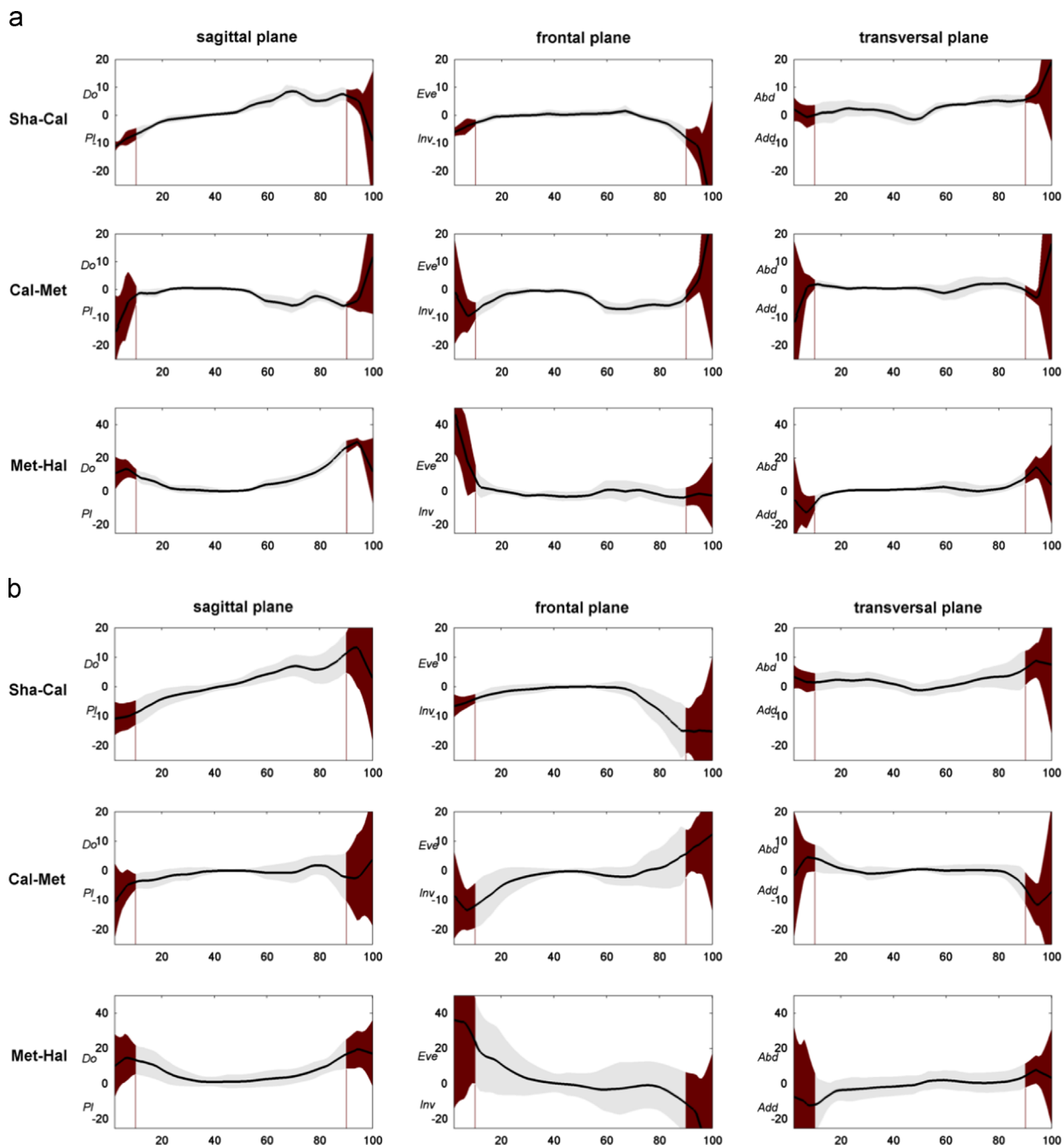


Fig. 5. (a and b). Joint rotations during the stance phase of walking for the 3 joints analyzed (Sha–Cal, Cal–Met, Met–Hal) in sagittal, frontal and transversal planes. Mean (solid line) plus and minus a standard deviation (gray) are reported for entire stance. Dark-red colored intervals are not included in HQS. a: 6 trials of 1 representative subject (subject 1). b: All 5 subjects, 6 trials each. (For interpretation of the references to color in this figure legend, the reader is referred to the web version of this article.)

A good ICP fitting is essential to calculate correct intersegment angles. Despite the robustness of rigid ICP to artifacts, it may still be prone to those point clouds that contain large holes, shown in Fig. 7c. Therefore the development of fitting algorithms that are even more robust to low data quality should be investigated in future research. The RMS error and percentage of fitting points between the reference and the dynamic measurement of each segment, were introduced to get an objective measure of the fitting quality. However, they give a first indication of the quality but it is not always straightforward to interpret them. This is further elaborated in [Supplementary appendix](#).

The present method is the first to be fully elaborated to obtain acceptable repeatability results. It is a semi-automatic method

which requires a rough indication of easy locatable landmarks during the segment selection step. This manual landmark selection is preferred over automatic selection, as the latter is not straightforward because of high inter-individual variability of foot anatomy (Liu et al., 2004; Witkowski et al., 2005). The influence of different raters indicating the landmarks is not expected to be of critical importance, but should be quantified in further research.

The hardware setup needs to be placed close to the subject's feet. This can influence their gait, and thus affect the measurements. Further improvement of 3D scanner systems should make it possible to place the scanners at a larger distance. On the other hand, having no markers placed on their feet, the subjects are able to walk freely, which has a positive effect on the measurements.

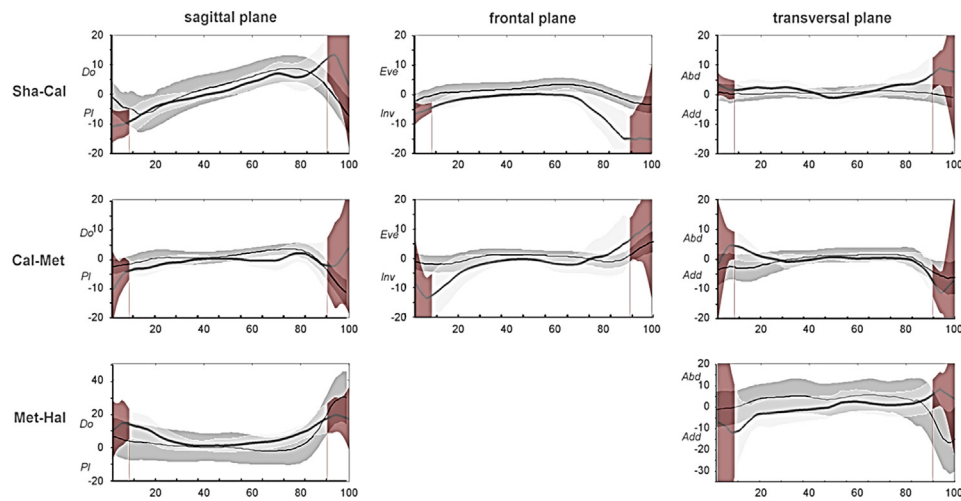


Fig. 6. Superimposition of present scan-based joint kinematics (light-gray, as in Fig. 5b) with corresponding patterns from marker-based kinematics with a similar multi-segmental model (dark-gray, (Leardini et al. 2007), with permission from the publisher).

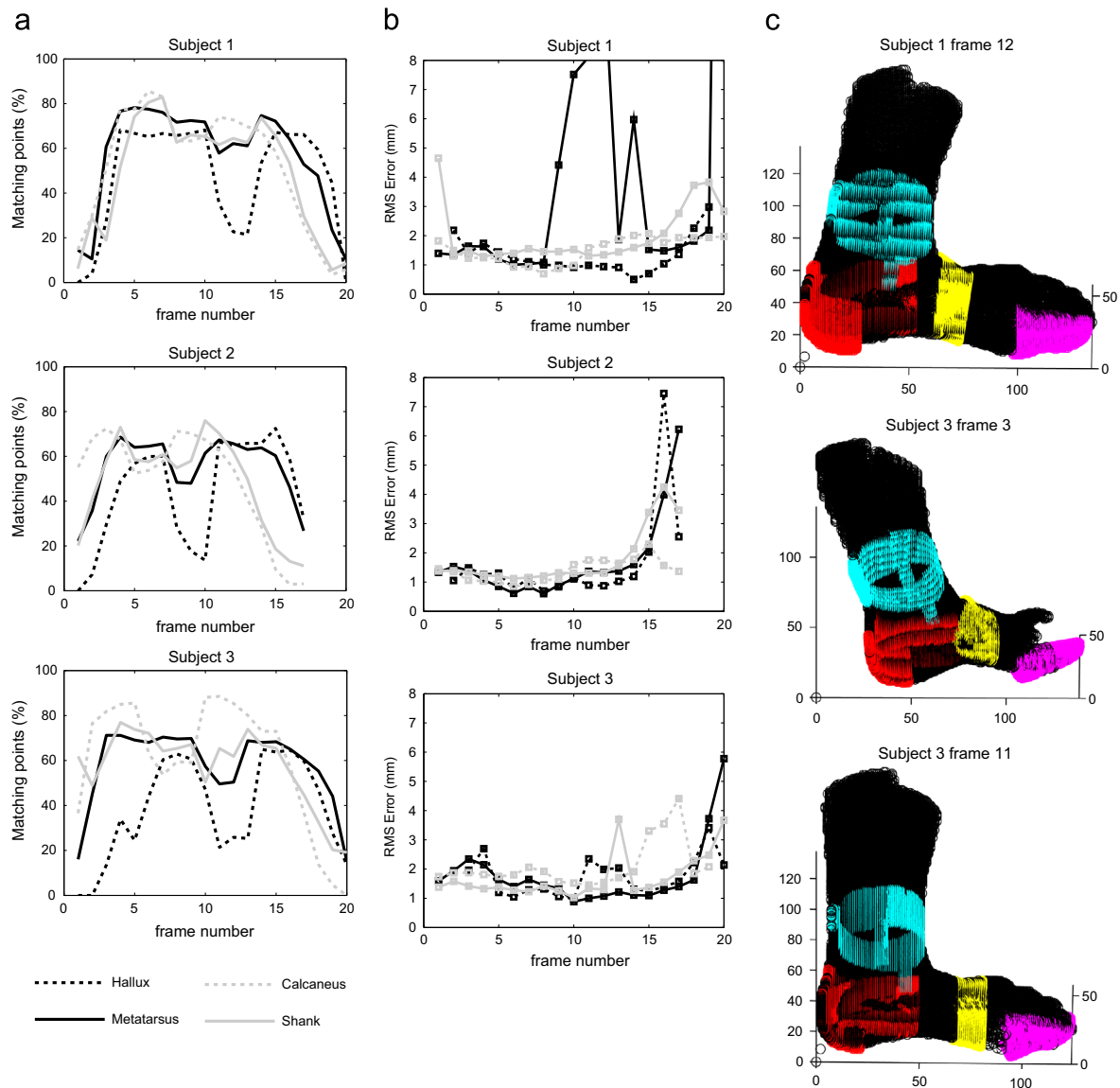


Fig. 7. (a–c). a: The matching data points between the reference segments and the dynamic measurements, in percentage values. This value is introduced because the RMS does not always give a good representation of the fitting quality. The drop in percentage of the hallux segment around frame 10 is due to the contralateral swinging leg which blocks the cameras. b: The root mean square (RMS) of the error values in mm of the fitting, for 3 subjects and segment in the different frames. For each subject, the first trial is shown. The error values outside HQS are higher. We also notice higher values for the metatarsus segment in subject 1. c: The matching of the different segments for 3 frames of subject 1 and 3. In subject 3 there is a misfit in the hallux segment. In frame 3 it shows an incorrect dorsiflexion of the hallux segment. In frame 11 there is an erroneous adduction of the hallux segment due to a low number of data points. In subject 1, there also is a low number of data points, but the fitting is much better.

This research mainly shows the possibilities of a multi-segment model in D3Dscanning, but no work has been done yet to optimize the segment selection. We opted for four segments. However, in subsequent studies the clinically interesting midfoot segment for example could also be included, provided that its shape characteristics are sufficiently recognizable in dynamic situations. A next step is to modify the segment borders to more anatomically-based segment shapes. Finally, the idea of automatic segment selection, based on the dynamic scans (instead of purely on the static scan as the current study describes), is very attractive but challenging. Automatic segment delineation could be done by adding an optimization step where each segment is evaluated for its rigidity during the motion. Nevertheless, from our experience, we would expect that any of these improvements in segment selection will only have limited impact on the resulting joint rotations.

6. General conclusions and prospects

In conclusion, the current study demonstrates the feasibility and limitations of calculating multi-segment foot kinematics during stance phase using D3Dscanning. The technique is limited to walking because of the frequency of data acquisition, and to stance phase because of the field of view. Due to relatively low quality of the acquired data during the first and last 10% of stance, these data were excluded. Hence, well-known motions outside HQS, such as the plantar flexion motion of the calcaneus after heel strike and in late propulsion, as well as the extensive toe dorsiflexion in late stance, are not calculated. The influence of lower scan quality is seen also in the typical hourglass pattern of the SD ranges. These problems will largely be solved when D3DScanners that can achieve a higher scan frequency become available. This is an upcoming development.

With this in mind, D3DScanning opens possibilities in kinematic foot analysis. The main advantages over conventional marker-based techniques are the easy and quick measurements without rater-dependency. Furthermore, the technique also allows for the calculation of a variety of other parameters, such as shape deformation and segment delineation in future research. The proposed calculation of joint rotations through a shape-based multi-segment foot model is a radically different approach to others, and it is up to future work to make a thorough validation. The first tests on five subjects show a good repeatability during HQS ($1^\circ < \text{WSSD} < 2.5^\circ$ for most joints), and the joint rotations are in line with previously published results. With a cost price reduction of scanner systems, which can be expected for the next few years, D3DScanning can offer an option to implement the calculation of foot kinematics in clinical practice.

Conflict of interest statement

None.

Acknowledgments

This work was supported through a grant of the Agency for Innovation by Science and Technology in Flanders (IWT: TETRA IWT no. 100402) in the international Era-SME program, with partners KU Leuven and Sports Medicine Tübingen. We thank also our supporting companies Materialise, V!GO, RSscan International, Orthopedics Van Haesendonck, Custom8, and Sprofit orthopedics. None of the supporting companies had any influence on results reported in this article. Furthermore we express

our thanks towards Jacob Wilm for his documented implementation of the rigid ICP algorithm, to our partners from KU Leuven: Ilse Jonkers, Friedl De Groote and Koen Peeters for their input, our partners from Sports Medicine Tübingen: Clemens Planck, Timo Schmeltzpfenning and Stefan Grau, and to Mobilab colleagues: Veerle Creylman, Luiza Muraru and Marijke Huybrechts for writing assistance, and Wim Dewindt, Helga Vertommen and Eveline De Raeye for general support.

Appendix A. Supplementary material

Supplementary data associated with this article can be found in the online version at <http://dx.doi.org/10.1016/j.jbiomech.2014.06.010>.

References

- Baker, R., 2006. Foot models for clinical gait analysis. *Gait Posture* 23, 399–400.
- Blenkinsopp, R., Harland, A., Price, D., Lucas, T., Roberts, J., 2012. A Method to Measure Dynamic Dorsal Foot Surface Shape and Deformation During Linear Running Using Digital Image Correlation. In: Proceedings of the 9th Conference of the International Sports Engineering Association (ISEA).
- Coudert, T., Vacher, P., Smits, C., Van der Zande, M., 2006. A method to obtain 3D foot shape deformation during the gait cycle. In: Proceedings of the 9th international symposium on the 3D analysis of human movement.
- Davis, I., 2004. How do we accurately measure foot motion? *J. Orthop. Sports Phys. Ther.* 34 (9), 502–503.
- De Mits, S., Segers, V., Woodburn, J., Elewaut, D., De Clercq, D., Roosen, P., 2012. A clinically applicable six-segmented foot model. *J. Orthop. Res.* 30 (4), 655–661.
- Deschamps, K., Staes, F., Roosen, P., Nobels, F., Desloovere, K., Bruyninckx, H., Matricali, G.A., 2011. Body of evidence supporting the clinical use of 3D multi-segment foot models: a systematic review. *Gait Posture* 33, 338–349.
- Fritz, B., Schmeltzpfenning, T., Plank, C., Grau, S., 2011. Influencing variables on 3D measured foot length during gait in children and adolescents. *Footwear Science* 3 (1). In: Proceedings of the Tenth footwear Biomechanics Symposium, pp. S53–S54.
- Fritz, B., Schmeltzpfenning, T., Plank, C., Hein, T., Grau, S., 2013. Anthropometric influences on dynamic foot shape: measurements of plantar three-dimensional foot deformation. *Foot Sci.* 5 (2), 121–129.
- Jezerek, M., Mozina, J., 2009. High-speed measurement of foot shape based on multiple-laser-plane triangulation. *Opt. Eng.* 48.
- Kimura, M., Mochimaru, M., Kanade, T., 2011. 3D measurement of feature cross-sections of foot while walking. *Mach. Vis. Appl.* 22, 377–388.
- Kjer, H.M., Wilm, J., 2010. Evaluation of surface registration algorithms for PET motion correction (Master thesis). Technical University of Denmark, Kongens Lyngby.
- Kouchi, M., Kimura, M., Mochimaru, M., 2009. Deformation of foot cross-section shapes during walking. *Gait Posture* 30, 482–486.
- Leardini, A., Benedetti, M.G., Berti, L., Bettinelli, D., Nativio, R., Giannini, S., 2007. Rear-foot, mid-foot and fore-foot motion during the stance phase of gait. *Gait Posture* 25, 453–462.
- Liu, X., Wangdo, K., Drerup, B., 2004. 3D characterization and localization of anatomical landmarks of the foot by FastSCAN. *Real-Time Imaging-Spec. Issue Imaging Bioinf.: Part III* 10 (4), 217–228.
- Long, J.T., Eastwood, D.C., Graf, A.R., Smith, P.A., Harris, G.F., 2010. Repeatability and sources of variability in multi-center assessment of segmental foot kinematics in normal adults. *Gait Posture* 31, 32–36.
- McGinley, J.L., Baker, R., Wolfe, R., Morris, M.E., 2009. The reliability of three-dimensional kinematic gait measurements: a systematic review. *Gait Posture* 29, 360–369.
- Mündermann, L., Corazza, S., Andriacchi, T.P., 2010. Markerless human motion capture through visual hull and articulated ICP. *Int. J. Comput. Vis.* 87, 156–169.
- Nester, C., Jones, R.K., Liu, A., Howard, D., Lundberg, A., Arndt, A., Lundgren, P., Stacoff, A., Wolf, P., 2007. Foot kinematics during walking measured using bone and surface mounted markers. *J. Biomech.* 40, 3412–3423.
- Okita, N., Meyers, S.A., Challis, J.H., Sharkey, N.A., 2009. An objective evaluation of a segmented foot model. *Gait Posture* 30, 27–34.
- Schmeltzpfenning, T., Plank, C., Krauss, I., Aswendt, P., Grau, S., 2009. Dynamic foot scanning. A new approach for measurement of the human foot shape while walking. *Footwear Science* (1). In: Proceedings of the Ninth Footwear Biomechanics Symposium, pp. S28–S30.
- Schmeltzpfenning, T., Plank, C., Fritz, B., Aswendt, P., Grau, S., 2011. 3D dynamic behaviour of foot structure may provide additional information for last design. *Footwear science* 3(1). In: Proceedings of the Tenth footwear Biomechanics Symposium, pp. S147–S148.
- Schwarz, M.H., Trost, J.P., Wervy, R.A., 2004. Measurement and management of errors in quantitative gait data. *Gait Posture* 20, 196–203.
- Simon, J., Doederlein, L., McIntosh, A.S., Metaxiotis, D., Bock, H.G., Wolf, S.I., 2006. The Heidelberg foot measurement method: Development, description and assessment. *Gait Posture* 23, 411–424.

- Van den Herrewegen, I., Cuppens, K., Broeckx, M., De Raeve, E., Vertommen, H., Mertens, M., Peeraer, L., 2012. Foot inter-segment angles and rotation axes based on dynamic 3D surface point clouds. *J. Biomech.* 45 (S1), S197.
- Wand, M., Adams, B., Ovsjanikov, M., Berner, A., Bokeloh, P., Jenke, P., Guibas, L., Seidel, H.P., Schilling, A., 2009. Efficient reconstruction of non-rigid shape and motion from real-time 3D scanner data. *ACM Trans. Gr.* 28 (2) (Article no. 15).
- Witkowski, M., Rapp, W., Sitnit, R., Kujawska, M., Vander Sloten, J., Haex, B., Bogaert, N., Heitmann, K., 2005. Automatic anatomical structures location based on dynamic shape measurement. In: *Proceeding of SPIE International Congress on Optics and Optoelectronics* (5959), pp. 78–86.